THERMAL MAPPING OF COASTAL WATERS

P. Lohmann
Institute of Photogrammetry and Engineering Surveys
University of Hannover
Federal Republic of Germany
Commission VII, WG VII/I

1. ABSTRACT

Coastal waters are known as areas influenced by pollution not only by chemical but also by thermal inlets.
Hence the use of thermal infrared sensing techniques and the evaluation of its data becomes an important tool for maintaining the coastal environment. Quantitative evaluation of thermal data prerequisites the removal of instrumental and atmospheric errors masking the desired information.
This paper discusses different approaches for error correction. The obtained absolute accuracy of $\pm$ 0.2 ^{o}C promises the effective use of those data in preparing thematic maps, by using digital image processing and screening techniques.

2. INTRODUCTION

The special research project, SONDERFORSCHUNGSBEREICH 149, sponsored by the DFG (Deutsche Forschungsgemeinschaft) was engaged since 1974 with the application of Remote Sensing in Coastal Areas (Annual Reports of SFB 149), namely in an area called Jade Estuary at the German North Sea Coast (see Fig. 1).
Although parts of that area are defined as national parks the Jade Estuary represents the biggest German oil harbour going together with associated industry.
A 720 MW power plant is situated in this area which uses coastal waters for cooling purposes. This power plant alone changes coastal water up to 21 m^3/sec which is warmed up by ~ 10.7 K and returned to the coastal water, where it is mixed by tidal effects, which are in the order of up to 4 m height. In order to estimate the influence of this inlet thermal data of that area were acquired by using a multispectral scanner BENDIX M^2S and DAEDALUS DS 1240/1260. A number of ground truth data were collected in order to calculate inter alia for atmospheric absorption and emission as well as evaporation at the water surface. Ground truth thermal data were obtained by using bucket thermometers profiling the area of interest. In addition to water temperature readings atmospheric measurements of the vertical and horizontal distribution of air temperature and water vapour contents were performed using both measurements made by local vertical radioprofiles and helicopter flights. Instrumental errors were accounted for by laboratory calibration of scanners and thermometers.
Atmospheric corrections were calculated by computer programs including the LOWTRAN V computer code (KNEIZYS, F.X et al 1980) and other appropriate programs (LOHMANN, 1983).
Image processing and map production was done by the Hannover MOBI-DIVAH image processing system (DENNERT-MÖLLER et al 1982) and the cartographic section of the Hannover University.

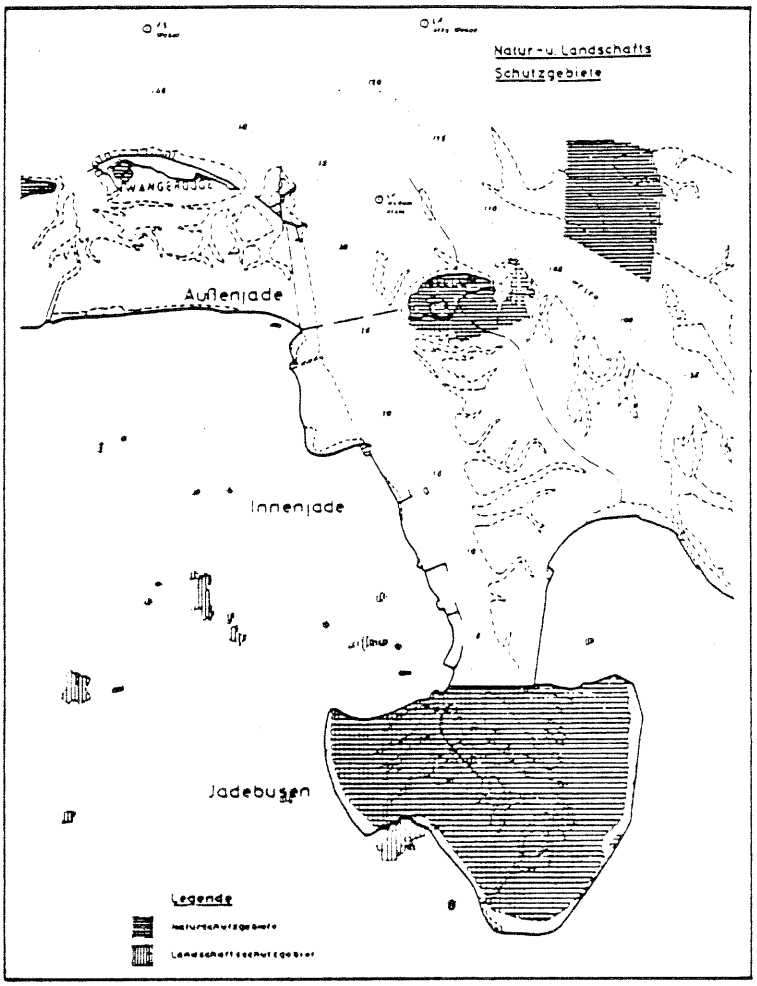

Fig. 1
Testarea 'Jade'

3. PREPROCESSING OF THERMAL IMAGERY

The calibration of the BENDIX M^{2}S was performed by scanning a system of two coupled ADKIN-Blockbodies adjustable within a range of - 20 °C to + 65 °C. These Blockbodies (BB) have a maximal emission at a wavelength of 11,5 µm and the usable field of view for laboratory calibration was ± 40 °C (STAETTER, 1981). The calibration graphs of the internal BB of the BENDIX-scanner (see Fig. 2), shown at different scan rates, demonstrate the need of proper calibration for quantitative analysis of the data.
Analysis of the imagery obtained during laboratory calibration also showed a random noise up to 0.71 °C perpendicular to the scan direction which has to be considered for. Fig. 3 shows the variation of the video-values perpendicular to scan direction. Analyzing its appropriate normalized auto covariance. (Fig. 4) it can be seen, that there is no auto correlation and the process is stationary. Water bodies with generally low variation in temperature (signal) show the effect of this noise more distinct than other areas. However for quantitative evaluation this noise has to be accounted for.
The method used to correct for this error is based on regression analysis and was described in detail by EHLERS and LOHMANN, 1982. Fig. 5 shows the effect of using this algorithm. Because all corrections applied to thermal data to remove atmospheric effects are based on the values of the measured temperatures itself, the removal of such noise effects is a prerequisite for quantitative evaluation of thermal data.

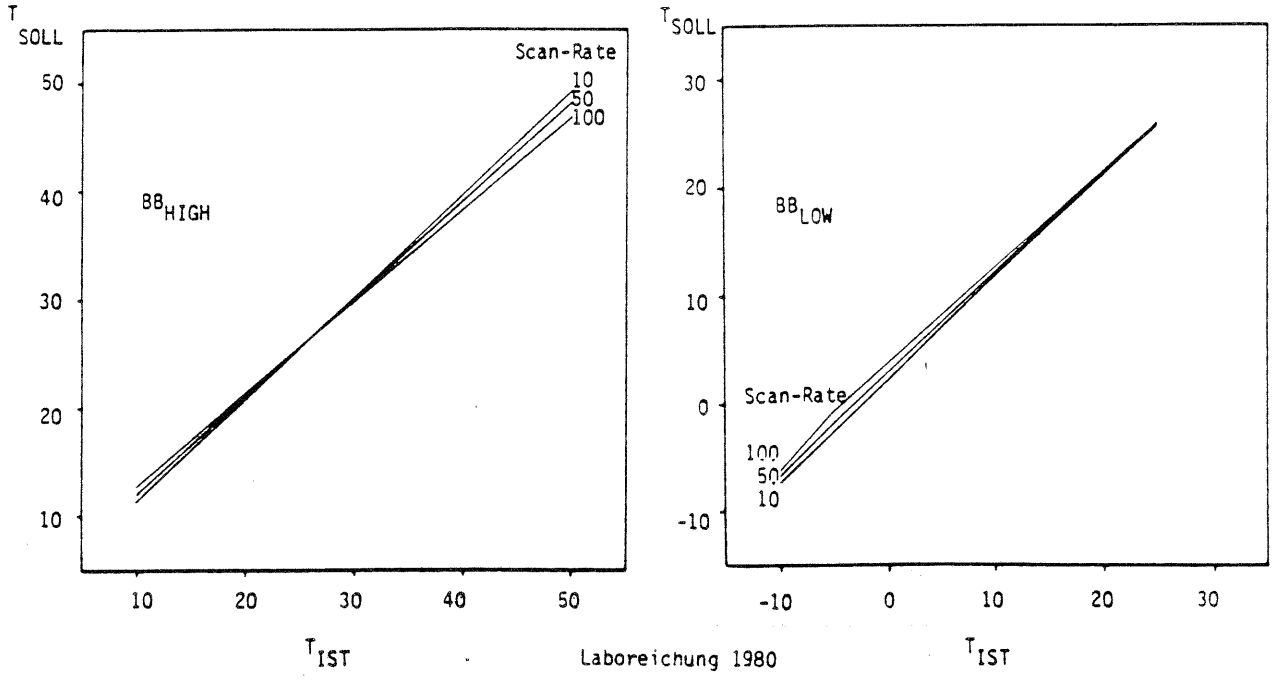

Fig. 2 Laboratory Calibration of BENDIX M^2S internal BB in 1980

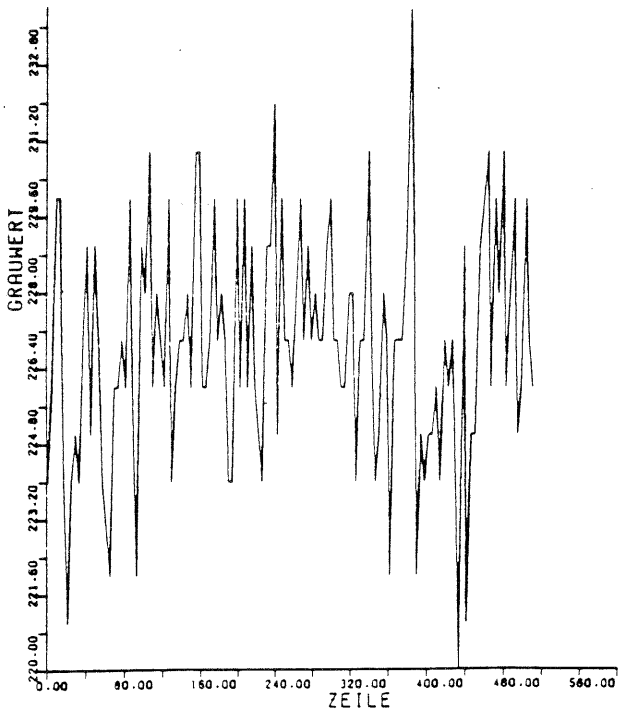

Fig. 3 Profile of video signal perpendicular to scan direction

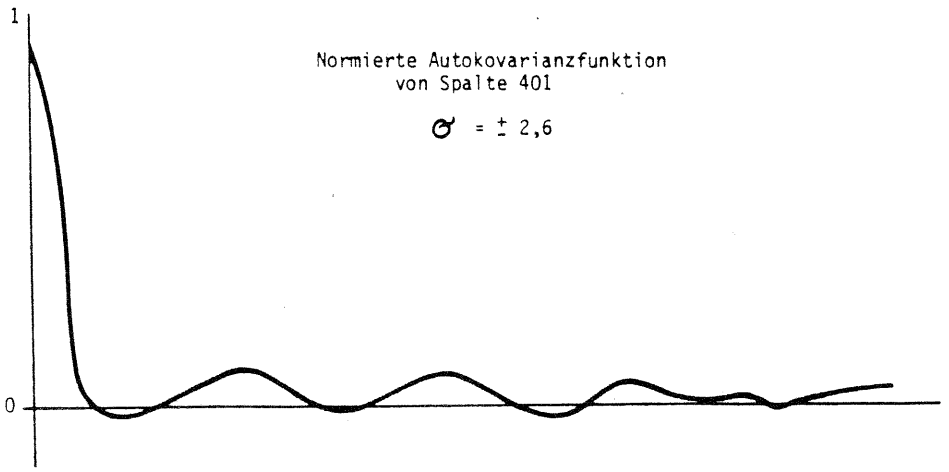

Fig. 4 Normalized auto covariance from Fig. 3

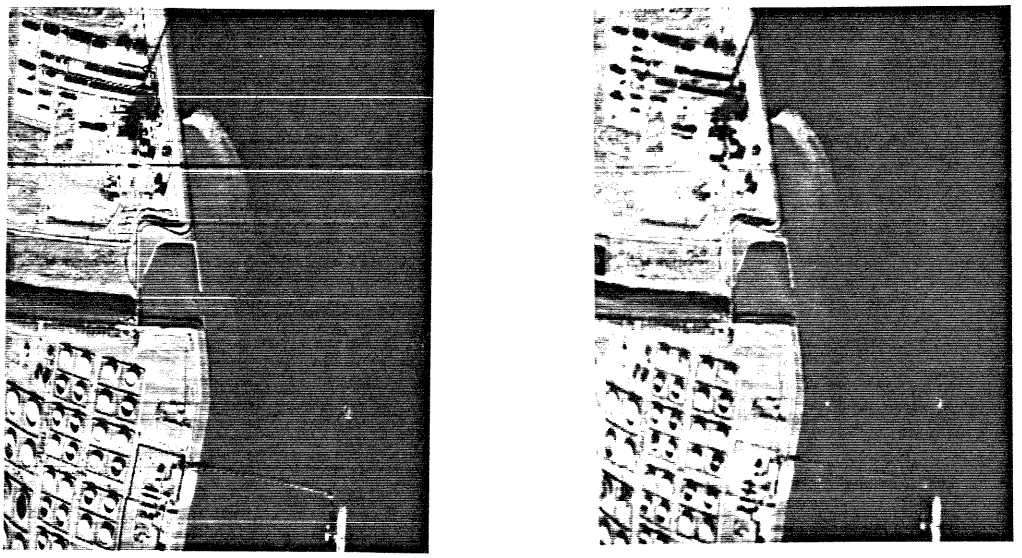

Fig. 5 Thermal image before and after filtering the scan line noise

4. ATMOSPHERIC CORRECTIONS

The measured radiation temperature at flight level H is distorted by the absorption and emission of the intervening atmosphere. Besides this one has to take into account that the earth has a lower emissivity than an ideal black body. Therefore one part of the atmospheric radiation is reflected into the recording system. The measured radiation temperatures of water surfaces are generelly lower than those temperatures measured at 10 - 20 cm below the water surface, because of evaporation effects at the skin of the water surface. SAUNDERS, 1967 and HASSE, 1971 discussed this effect and presented formulas for the calculation of evaporation at water surfaces. The following procedures for the correction of

thermal imagery ignore these techniques because all approaches presented here are based on the use of bucket thermometer readings as reference which were taken at ~ 10 cm below the water surface.

4.1 Interpolation technique

The approach described here is based on the availability of intense ground truth measurements. Ground truth was performed using boats equipped with bucket thermometers profiling the area covered by the scanner flight. The temperature readings were corrected for instrument errors and interpolated for the time of overflight. These reference readings showed great differences compared to the remote measured temperatures in the order of 2 to 3 °C. Because of varying path length perpendicular to the flight direction the radiance temperatures were corrected using equation (1).

(1) $$I' = I \left(\frac{1}{\cos \theta}\right)^k$$

I' = corrected radiance
I = measured radiance
θ = scan angle
k = damping factor ($0 < k < 1$)

The value of k has to be determined analysing local radiance distributions with

(2) $$I = I_{\theta=0} \left(\frac{1}{\cos \theta}\right)^k$$

The remaining temperature differences compared to the reference temperatures were used to derive the coefficients of polynomial like (3) using least square methods.

(3) $$\Delta T = A_o + \sum_{i=1}^{n} A_i \, (T_s - \bar{T}_s)^i$$

where T_s = measured radiation temperature
$\bar{T}_s$ = arithmetric mean of radiation temperature readings of that area
i = degree of polynomial ($i = 1, 2, 3, 4$)

The polynomials were derived using 12 reference readings while 22 independent readings were used to check the accuracy. In general all polynomials regardless of their degree showed accuracies better than ± 0,2 °C, but for image processing reasons polynomials with a degree higher than 2 could not be used. They showed good results when applied to temperatures in the range of water temperatures, but for higher temperatures like land sites saturation of image densities occured because of extrapolation reasons. Table 1 summarises the obtained results together with the used polynomial.
Using the differences between bucket temperature readings and temperatures derived from scanner data, this method automatically accounts for the evaporation effect mentioned before.

Polynomials	obtained accuracy [°C]
$\Delta T = A_o + A_1 T_s$	$\pm$ 0.16
$\Delta T = A_o + A_1 T_s^2$	$\pm$ 0.16
$\Delta T = A_o + A_1 T_s^3$	$\pm$ 0.17
$\Delta T = A_o + A_1 T_s^4$	$\pm$ 0.19
$\Delta T = A_o + \sum_{i=1}^{2} A_i (T_s - \overline{T}_s)^i$	$\pm$ 0.14
$\Delta T = A_o + \sum_{i=1}^{3} A_i (T_s - \overline{T}_s)^i$	$\pm$ 0.14
$\Delta T = A_o + \sum_{i=1}^{4} A_i (T_s - \overline{T}_s)^i$	$\pm$ 0.19
$\Delta T = A_o + (\frac{1}{\cos \theta})^k T_s$	$\pm$ 0.21

Table 1 Used polynomials and obtained accuracy
(12 reference readings, 22 independent check points)

4.2 Calculation of atmospheric extinction and reflection at the water surface

According to DESCHAMPS, 1977 the difference between the apparent radiation temperature $T_s(H)$ as measured at flight level H and the true radiation temperature T^s can be expressed by the approximation (4) which is composed by the error due to absorption and emission of the atmosphere (5) and the error due to 'non-blackness' of the surface (6)

(4) $\Delta T = \Delta T_{reflection} + \Delta T_{extinction}$

(5) $$\Delta T_{extinction} = \frac{\int_{\lambda_1}^{\lambda_2} \phi_\lambda \int_{H}^{0} (L_\lambda (T_L(h)) - L_\lambda (T_s(0))) \frac{\partial \tau_\lambda}{h} \, dh \, d\lambda}{\int_{\lambda_1}^{\lambda_2} \phi_\lambda \frac{dL(T)}{d\overline{T}} \, d\lambda}$$

(6) $$\Delta T_{reflection} = \frac{\int_{\lambda_1}^{\lambda_2} \phi_\lambda (1 - \varepsilon_\lambda) (A_\lambda - L_\lambda (T)) \, d\lambda}{\int_{\lambda_1}^{\lambda_2} \phi_\lambda \frac{dL_\lambda (\overline{T})}{d\overline{T}} \, d\lambda}$$

where ϕ_λ = spectral detectivity of the instrument

L_λ (T) = spectral radiance at temperature T according to Planck's law

T_s (0) = apparent surface temperature (altitude 0 m)

T_L (h) = air temperature at hight h

τ_λ = spectral transmission of the atmosphere

A_λ = spectral irradiance of the atmosphere

ε_λ = spectral emissivity of the surface

For the determination of (5) an iterativ approach was used as discussed in detail by LOHMANN, 1983. Equation (5) requires the knowledge of the vertical distribution of temperature and water vapour of the atmosphere in order to calculate the vertical gradient of the spectral transmission of the atmosphere as proposed by KONDRATYEV, 1972. The influence of Ozon absorption in the wave-length interval between 8 and 13 µm was found to be of minor importance up to flight altitudes of 5 km. Vertical profiles of temperature and humidity as measured by meteorological stations close to the test site were combined with own measurements especially in the lower part of the atmosphere. Soundings made by helicopter-flights were found to be systematic erroneous due to turbulence effects caused by the helicopter itself. Fig. 6 shows a graphic presentation of tables calculated from radiosonde-data taken into account different viewing angles of the instrument, and different flight altitudes.

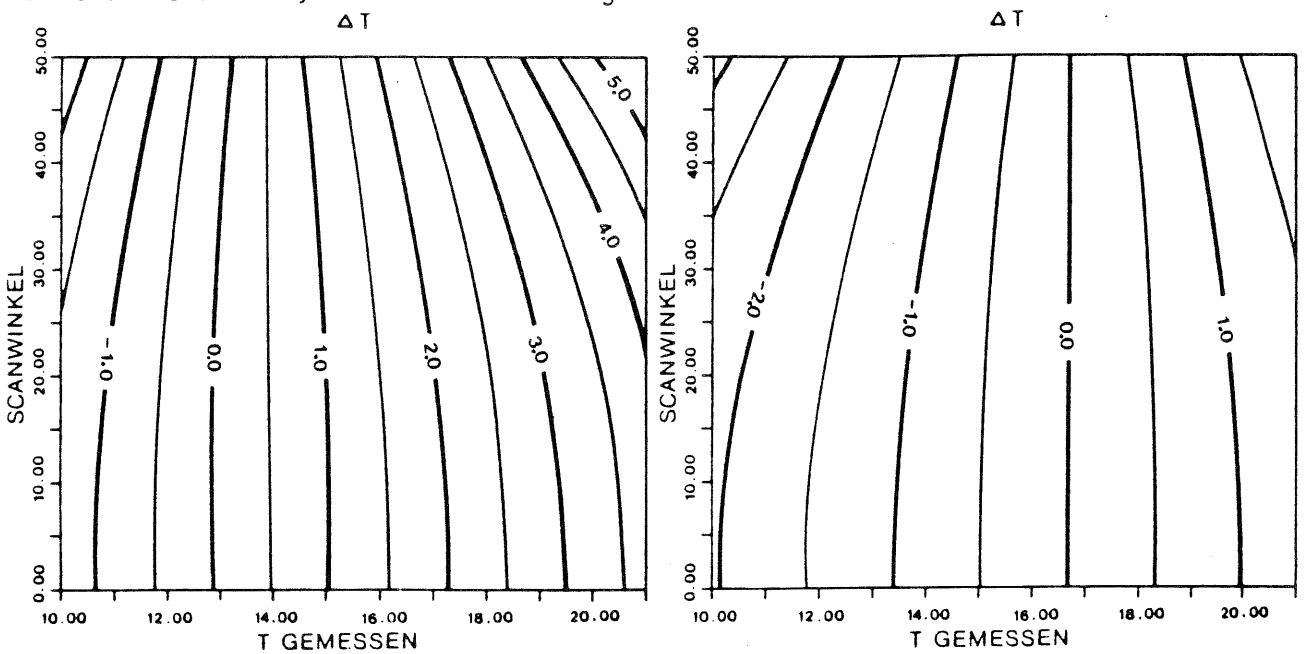

Fig. 6 $\Delta T_{extinction}$, calculated for a flight altitude of 3600 m (left) and 1600 m (right) using radiosonde-data of Hannover meteorological station 12.08.1976

For the determination of (6) the measurement of the numerator is difficult for practical purposes, BUETTNER and KERN, 1965 and LORENZ, 1973. Therefore the spectral dependance of the emissivity of water was committed that is to say water is considered to be a 'gray-body'. The spectral irradiance was calculated using data sets combined by model data from LOWTRAN V, (KNEIZYS et al 1973) and radiosonde-data as before. Fig. 7 shows as an exemple the global irradiance calculated for different zenith angles and Fig. 8 shows the values of (6) for different emissivities. Using the temperature readings of only a few reference points to select the appropriate emissivity the correction (6) can be applied for the whole thermal image. Again by using a 'Pseudo-emissivity' the effect of evaporation at the water surface is included by this method.

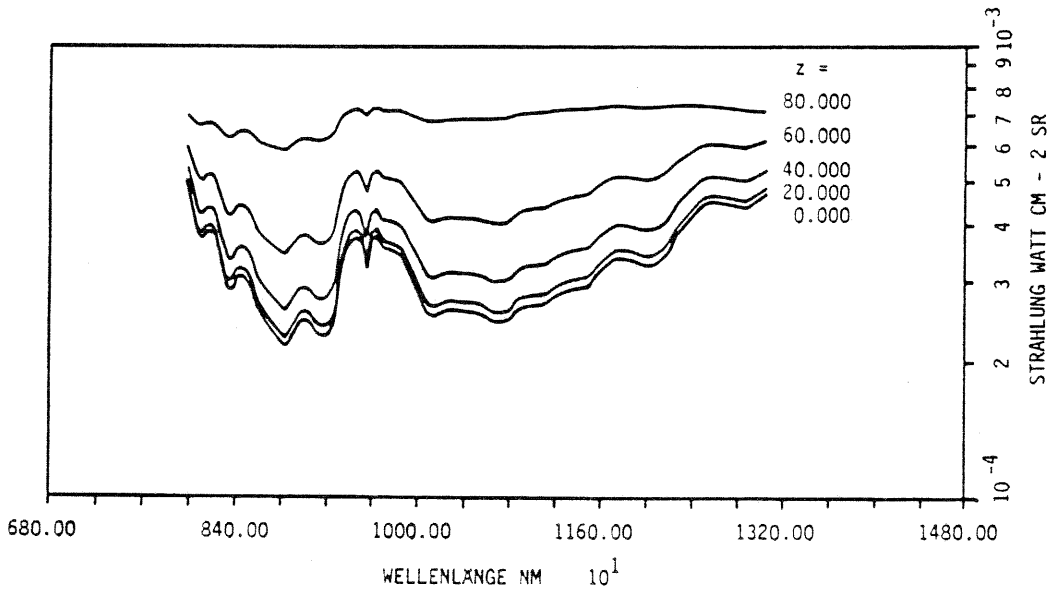

Fig. 7 Spectrum ofcalculated incomming radiation for different zenith angles (calculated with LOWTRAN V-data and radiosonde-data of Hannover, 12.08.1976)

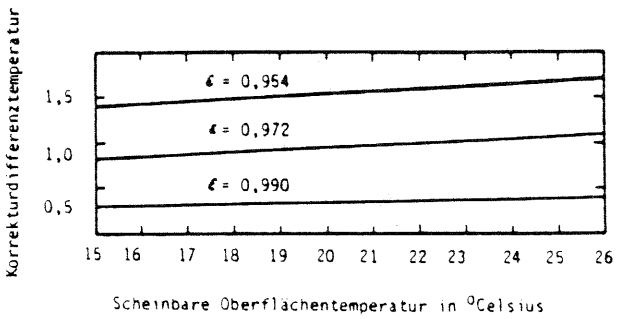

Fig. 8 Correction of reflection for different 'emissivities'

The total correction applied to the image can be seen by looking to Fig. 9, where the difference between the original scene, the filtered and atmospheric corrected image is presented. The scan angle dependence of the used correction can clearly be identified. Table 2 gives a summary of the obtained accuracies.

Date	Altitude m	Instrument	Original data		Corrected data	
			syst. error	variance	syst. error	variance
			°C	°C	°C	°C
12.08.76	1600	BENDIX	2.7	0.6	- 0.1	0.2
12.08.76	3600	BENDIX	2.4	0.5	0.4	0.3
28.10.81	900	BENDIX	2.5	0.4	0.3	0.2
28.10.81	900	DAEDALUS	2.6	0.3	0.4	0.2
28.10.81	600	BENDIX	1.9	0.3	0.2	0.2
28.10.81	600	DAEDALUS	2.0	0.4	0.3	0.2
28.10.81	300	BENDIX	1.9	0.3	0.1	0.3
28.10.81	300	DAEDALUS	2.0	0.3	0.1	0.3

Table 2 Accuracies obtained using atmospheric corrections

5. PRESENTATION OF RESULTS

The presentation of results depends mainly on existing hardware to produce hardcopies of the imagery. The easiest way consists in printing image maps on a line printer, but the number of levels to be printed in a single print is limited due to hardware restrictions.
Another way of presenting results is the output of temperatures in form of isolines. This is a common method, but it has the disadvantage that a loss of information for the interpretation must be taken into consideration while going from image data to line-(graphic) data.
If a film writer can be used the corrected image can be written to film with varying density according to varying temperatures. The exact interpretation of temperatures is difficult, because the human eye can only differentiate small numbers of grayvalues. If a density sliced black and white output is used the interpretation becomes easier but again the number of steps in limited by the human eye.

Color coded and density sliced output presents the most favourable output for the human eye because its ability to distinguish colors much better than graytones. But this method is linked with high costs especially if a number of identical outputs are required. For printing purposes the colorfilm has to be color separated, screened and copied to printing plates. An efficient way of producing printing sheets is to use electronic screening as it is realized in film writers like the HELL CHROMAGRAPH. Because these instruments are expensive a computer program was written to screen images for printing preparation by using digital image processing.

Fig. 10 Enlargement of a digital screened image

Fig. 10 shows an enlargement of a digital screened color separate, which was used to prepare a thematic map which is shown in Fig.11. Screening angle and the number of picture elements per cm were derived from SCHMIDT, 1975 and are shown in Table 3.

Color	Number of picture elements per cm	Screening Angle	Difference in Angle
Cyan	62,5	51,3 ^{o}	- 35,4 ^{o}
Magenta	54,7	15,9 ^{o}	- 15,9 ^{o}
Yellow	57,1	0,0 ^{o}	- 18,4 ^{o}
Black	63,3	- 18,4 ^{o}	

Table 3 Screening data

The values of SCHMIDT allow fitting tolerances between the different color separations of up to 1,4 ^{o} without having problems with moiré-effects. The color separates were produced using an OPTRONICS P1700 system, which is based on a rectangular writing pattern.

CONCLUSION

Both correction approaches showed useful results which are in the order of 0.1 to 0.3 ^{o}C. A prerequisite for the application of atmosheric corrections is the filtering of the original scene due to scanline noise and the prior application of laboratory calibrations. Because of the additive and multiplicative nature of the atmosheric contribution the interpolation technique showed satisfactory results. The disadvantage of this method is the need for extensive ground truth measurements going together with a high

amount of logistics. Therefore the second approach is likely to be more efficient especially if meteorological stations are close to the testsite. It requires only a small ammount of ground truth, although the computation effort is much higher.
The presentation of results is considered to be optimal in form of colored thematic maps. The use of digital screening techniques can reduce the costs for printing preparation, especially if a great number of different maps have to be produced. Existing geographic and graphic information from base maps can be combined with the thematic temperature information in order to provide interpreters with a maximum of information.

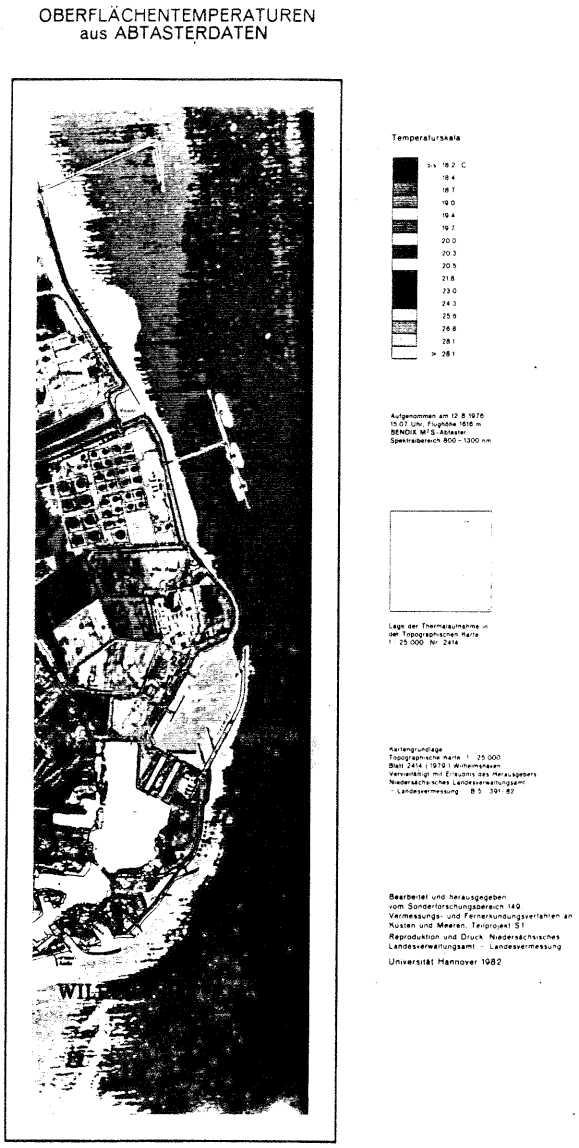

Fig.11 : Thermal Map of the JADE - Estuary

LITERATURE

BUETTNER, K.J.K., KERN, C.D.: The determination of infrared emissivities of terrestrial surfaces. Journal Geophys. Res., Vol. 70, No. 6, 1965

DESCHAMPS, P.Y.: Télédétection de la température de la surface de la mer par radiométric infra rouge. Thèse de Doctorat d'Etat, Université de Lille, N^{O} 376, 1977

DENNERT-MÖLLER, E.M., EHLERS, M., KOLOUCH, D., LOHMANN, P.: Das digitale Bildverarbeitungssystem MOBI-DIVAH, BuL 50, pp. 201-203, 1982

EHLERS, M., LOHMANN, P.: Digitale Bildverbesserung von verrauschten Abtasterdaten, BuL 5/1982

HASSE, L.: The sea surface temperature deviation and the heat flow at sea-air interface. Boundory Layer Meteorology, 1, 1971

KNEIZYS, F.X. et al: Atmospheric Transmittance/Radiance: Computer Code LOWTRAN V. Environmental Research Paper No. 697, AFGL-TR-80-0067, Hauscom., Mass., 1980

KONDRATYEV, K.Y.: Radiation processes in the atmosphere. WMO, Genf, No. 309, 1972

LOHMANN, P.: Digitale Korrektur von Thermalaufnahmen aus mittleren Höhen von küstennahen Wasserflächen, Int. Archiv f. Photogrammetrie Hamburg 1980

LOHMANN, P.: Untersuchungen zur digitalen Auswertung und Korrektur von thermalen Abtasterdaten von küstennahen Wasserflächen, Wissenschaftliche Arbeiten der Fachrichtung Vermessungswesen der Universität Hannover, ISSN0174-1454, Nr. 123, Hannover 1983

LORENZ, D.: Die radiometrische Messung der Boden- und Wasseroberflächentemperatur und ihre Anwendung insbesondere auf dem Gebiet der Meteorologie, Z. Geophys., 39, 1973

SFB 149: Annual Reports, wiss. Arbeiten der Fachrichtung Vermessungswesen der Universität Hannover 1974 - 1983, ISSN0174-1454, Hannover

STAETTER, R., WACKER, F.: Calibration Data for BENDIX M^{2}S Scanner, Internal Report, DFVLR, 1981

SCHMIDT, H.: Ein Beitrag zur mehrfarbigen Rasterreproduktion unter besonderer Berücksichtigung großformatiger Kopierraster und einer optischen Kombination zwischen Rasterwinkelung und Rasterwerten, Dissertation, Bonn, 1975

SAUNDERS, P.M.: Aerial Measurement of Sea Surface Temperature in the Infrared, J. of Geophys. Res., Vol. 72, No. 16, 1967